Laser-induced forward transfer of conductive screen-printing inks

P. Sopeña[1,2], J. M. Fernández-Pradas[1,2], P. Serra[1,2]*

[1] Applied Physics Department, Universitat de Barcelona, Martí i Franquès 1, 08028, Barcelona, Spain.

[2] Institute of Nanoscience and Nanotechnology (IN2UB), Universitat de Barcelona, Av. Diagonal 645, 08028, Barcelona, Spain.

*corresponding author. E-mail: pserra@ub.edu

Abstract

Laser-induced forward transfer (LIFT), unlike inkjet printing, presents few constrains concerning ink viscosity or loading particle size. This is clearly favorable for printed electronics applications, since high solid content inks, such those of screen printing, can be thus transferred in a digital fashion. In this work we propose a study of the transfer mechanisms during the LIFT of a commercially-available silver screen printing ink.

The printing of single voxels on glass through the variation of pulse energy and donor-receiver gap reveals a linear dependence of voxel volume respect pulse energy for low energies and small gaps. The analysis of the transfer dynamics demonstrates that for the entire range of analyzed conditions the deposit takes place through bubble contact with the receiver.

The printing of lines through variation of the overlap between successive voxels reveals that under none of the analyzed conditions we obtain uniform continuous lines through single scan: the lines always show scalloping, bulging, or discontinuities. These defects are a consequence of the modification of the donor film morphology induced by previous pulses in the line, which makes the transfer dynamics unstable. A final multiple scan approach proves the feasibility of the technique for printing uniform stable lines.

Keywords

laser printing, laser forward transfer, screen printing ink, printed electronics

1. Introduction

In printed electronics, direct-write techniques are emerging as interesting alternatives to more conventional techniques such as flexography, gravure or screen printing, which rely on the use of rolls and stencils [1,2]. The demand for digital techniques has risen in the last years thanks to their compatibility with short production runs, customization and defect repair. This is accomplished by entering user-designed patterns into a computer which translates the input information into a fully printed circuit by means of a printing device. Thus, production is much more accessible and affordable since no permanent support (rolls or stencils) for the pattern is required. Nowadays, inkjet printing (IJP) is the most widely extended digital technique in printed electronics [3]. In IJP droplets are ejected on-demand from a cartridge through an output nozzle. In order to print the desired material, the rheology of the employed ink has to be properly formulated to avoid nozzle clogging or head contamination issues [4]. Thus, the range of printable viscosities is limited to 1-10 mPa·s and the particle size must be around $1/100^{th}$ smaller than the nozzle output diameter [5,6]. Generally, this leads to inks with low solid content, typically lower than 20% [7,8], which can result in deposits with not enough material to grant that the printed features meet the aimed properties. For example, in the case of conductive inks, the typical sheet resistance of an inkjet printed line is of the order of 1 Ω/□, too high to be used as an interconnect [7,8].

High solid content inks are desirable in printed electronics applications since, for the same volume of deposited liquid ink, more solid material is finally contained in the printed feature. From the available commercial inks, screen printing (SP) inks show the highest solid contents, around 60-70% [7,9] which, besides the large dispersion in particle size (between hundreds of nanometers to tens of microns), result in high ink viscosities (10^2 to 10^6 mPa·s) [10]. These properties lead to improved performance for the printed feature. In consequence, in the case of conductive inks, sheet resistances below 50 mΩ/□ are easily achieved [7,8]. Moreover, their extended use makes them easily available and cost-effective [11]. However, in order to be printed through the SP meshes, these inks need to exhibit, in addition to the high viscosity already mentioned, a thixotropic behavior, which makes them in turn unprintable using IJP technology [6,10]; such behavior is due to the strong interaction between the particles loading the ink [12]. An alternative to IJP that allows printing SP inks in a digital fashion is laser-induced forward transfer (LIFT) [13].

In LIFT a few microns thick film of ink is extended on a transparent donor substrate which is placed facing the receiver substrate at a relatively small gap. A pulsed laser beam is then focused on the donor film so that a tiny fraction of material is projected forward. The laser pulse energy is absorbed by the ink, and this induces the formation of a cavitation bubble [14,15], which expansion and further collapse result in a jet that propels away the donor film. As this jet reaches the receiver substrate a droplet of ink is deposited [16]. Since LIFT is a nozzle-free printing technique there are almost no limitations on the rheology of the ink to print, being able to transfer a wide range of viscosities (1-10^6 mPa·s) and particle sizes (from nano- to micrometric) [17-23]. Even non-Newtonian inks can be successfully transferred, which is otherwise impossible using IJP heads [24-28].

In this work we carry out a study of the LIFT technique for printing commercially-available conductive SP inks with high solid content. First, we print single voxels at different pulse energies and gaps to determine how these parameters affect the features morphology. Later, in order to obtain continuous lines that could be used as interconnects in electronics applications, we vary the overlap between adjacent spots, finding the conditions leading to the most stable and uniform lines. The study is also aimed at achieving a better understanding of the transfer dynamics, for which we analyze it through time-resolved imaging. The imaging analysis is not only focused on liquid transfer during single voxel printing, but also during line printing, which allows to unveil the effect of previous laser pulses on each transfer event. The observed behavior correlates well with the printing experiments, though it reveals a liquid ejection dynamics substantially different from that typical of Newtonian low-viscosity inks.

2. Experimental

Laser direct-write system

In order to carry out the experiments we used a diode-pumped ytterbium fiber laser (Rofin Powerline F20 Varia). The laser worked at the fundamental wavelength (1064 nm) with a pulse width of 100 ns. The beam had a Gaussian beam intensity profile with a maximum energy of 800 μJ and a repetition rate which ranged from 2 kHz to 1 MHz. This laser unit was furnished with a galvanometric mirror head which allowed scanning the beam along a square surface of 6×6 cm^2 at speeds ranging from 10 mm/s to 5 m/s. A 100 mm f-theta lens after the galvo-unit focused the beam with a diameter of 40 μm at the sample plane, corresponding to the donor substrate-film interface.

Sample preparation and printing

We printed a commercial silver ink (Loctite EDAG PF 410 E&C) specifically designed for screen printing and flexible printed electronics applications. Its density was 2.5 g/cm^3, its particle size ranged between 0.3 and 10 μm, its nominal viscosity was 12.7 Pa·s and its solid content 74.1%. However, since SP inks are typically non-Newtonian, in order to characterize it we employed a dynamic shear rheometer (TA Instruments Discovery HR). Its viscosity versus the shear rate (Fig. 1) displays a shear-thinning behavior: the viscosity varies several orders of magnitude along the explored shear rate range, from 2 to 10^3 Pa·s (higher shear rates are not available with this rheometer). We prepared an 80 μm thick donor film by doctor-blading the Ag-SP ink onto a glass slide (Deltalab, 26×75 mm^2). The ink was later transferred onto a similar glass slide acting as receiver substrate placed at gaps ranging from 200 to 600 μm. Once we transferred the ink, the deposited voxels and lines were treated in a conventional oven at 120 ºC for 30 min as indicated by the manufacturer in order to enhance its functionality and reach a low enough resistivity (nominal resistivity of 37.5 μΩ·cm).

Imaging setup

Using a time-resolved imaging setup consisting of a pulsed light source, a CCD camera and a synchronization system, we observed the transfer dynamics. The light source was composed of a red LED (Thorlabs 630E) which light was gathered by a condenser of two lenses (focal lengths of 25.4 and 35 mm, respectively) and focused at the laser plane on the sample. The CCD camera (Thorlabs VC480Viewer), with an exposure time of 1 ms, was coupled to a 10× microscope objective in order to acquire the images of the transfer process. Both light source and camera were placed along the same optical axis in a shadowgraphy configuration at grazing incidence respect to the donor-receiver system. The laser beam was scanned along the image plane of the microscope objective and it was used for both triggering and printing events. The first pulse of the scanned line was sent to an external fast photodiode (Thorlabs DET10A/M Si detector) which, connected to a pulse generator (Stanford ResearchSystems, DG645), triggered the LED pulse and camera at controlled delays. Temporal resolution was achieved by means of a driver (PicoLAS LDP-V 10-70) that allowed an LED pulse duration of 100 ns. Using this method, we captured snapshots of the transfer process at different delays from the laser pulse.

Sample characterization

Line characterization was carried out using optical (Carl Zeiss, model AX10 Imager.A1) and confocal microscopy (Sensofar PLμ 2300).

3. Results and discussion

3.1 Voxel printing

We printed single voxels of Ag-SP ink on glass using different gaps and pulse energies at a constant separation between pixels of 500 μm. We tested five gaps, from 200 to 600 μm (in steps of 100 μm), varying the pulse energy accordingly in order to see its effect on the printed features. In Fig. 2 we can observe optical images of the voxels printed at different energies and a gap of 300 μm just after printing (wet droplets) and once removed from the oven (dry voxels). The printed voxels are quite large (clearly above 100 μm) in all cases, which is due to the relatively large gaps and thick donor films employed in the experiments. Although much smaller voxels would be desirable for the applications, in this study we have set conditions allowing the easy visualization of the transfer dynamics, which translates into both large gaps and features. It can be observed how the voxel diameter increases with energy, being 60 μJ the first explored energy at which material was transferred. From the optical microscope images in Fig. 2, wet droplets look very similar to dry voxels. However, a close inspection reveals that a morphological change from hemispherical droplets to cylindrical voxels occurred due to the evaporation of practically all the solvent within the first minutes after printing, which also resulted in a 15% reduction in the droplet radii. In view of the fast drying rate of the droplets after printing, all the morphological analysis was performed by characterizing the voxels, which corresponded to the remaining solid content on the receiver substrate. In Fig. 3a we plot the radius of the voxels versus pulse energy for all the gaps, and we observe how the radius follows an increasing trend with pulse energy, presenting a minimum diameter of around 160 μm. Also, it can be noted how the smallest feature is constant and does not depend on the gap, but the minimum energy (E_{min}) for printing does. Moreover, for a given printing energy, larger printed features can be obtained as the donor-receiver distance is reduced. This observation contrasts with previous experiments in which, for a certain pulse energy that led to transfer, the gap could be varied from a few hundred microns up to one millimeter with no significant droplet size variation [16]. However, in those studies a low-viscosity Newtonian ink was employed instead, which could account for the different behavior. Also, the described trend is relatively replicated in all the cases, indicating that similar results can be obtained using a wide range of gaps. Even though the minimum feature size is comparable to the ones obtained using SP [7,29], the resolution could be probably improved by using a tighter beam spot or a thinner donor film of a few tens of micrometers [30,31].

Using confocal microscopy we were able to measure the volume of the voxels (around 3 times smaller than that of the droplets due to solvent evaporation), which we plotted versus the pulse energy in Fig. 3b. Similar to the radius, the volume increases with pulse energy, with a minimum volume of around 50 pL which does not depend on the donor-receiver gap. This is beneficial from a technological point of view, since printing can be achieved with a high gap tolerance. The obtained cylindrical volumes range between 50 and 500 pL, with voxel heights between 2 and 5 μm. However, since all the solvent in the voxels evaporated, their surface is not completely smooth (as pointed out before, the voxels correspond to the remaining solid content in the dried ink), showing a mean surface roughness of 1 μm with peaks up to 5 μm above the voxel average height (probably corresponding to the big particles described in Section 2). These heights are much larger than the typical ones of IJP (~200 nm) and of the order of those common to SP [7,8,10]. For small gaps a linear relation between volume and energy is always observed, whereas the volume seems to saturate at high energies for larger gaps. In previous studies, a linear relation between the volume *V* of the deposited features and the pulse energy *E* was observed [32]. This has usually been described as:

$$V = K(E - E_0), \qquad (1)$$

where the proportionality constant *K*, and the threshold energy E_0 can be obtained from the linear fit. This law has proved to be valid in the LIFT of several low-viscosity liquids [14,30,32,33]. In this regard, we fitted eq. 1 to those points in Fig. 3b which were linearly aligned and both *K* and E_0 were obtained. The proportionality constant, which can be interpreted as the efficiency of the transfer process, decreases with the gap from 8.4 pL/μJ at 200 μm to 2.3 pL/μJ at 600 μm. On the contrary, the threshold transfer energy E_0 shows an increasing trend with the gap (from 25 to 170 μJ). Since the beam radius (ω) is the same in all the experiments, this means that the corresponding threshold fluence ($F_0 = E_0/\pi\omega^2$) also increases with the gap. This contrasts with other LIFT studies with Newtonian inks in which the threshold fluence F_0 was constant irrespective of the gap (and of the beam radius) and, as usually assumed, characteristic only of the liquid [14,16,33]. In the present case, however, we have different thresholds F_0 for the same ink. This apparent anomaly can be attributed to the non-Newtonian nature of the SP inks. For each different pulse energy the ink will be submitted to shear rates of different intensities which will follow a different evolution with time in each case. This will translate into different viscosities, and a different viscosity history (Fig. 1). Thus, it would be as if each laser beam with a different pulse energy was 'seeing' a liquid with a different viscosity. Under these circumstances, it should not be so surprising to find a different F_0 for each gap, even if working with the same ink. Therefore, the interpretation of F_0 as the fluence required to generate a bubble in the liquid typical of Newtonian inks [33] does not seem to apply in this case.

3.2 Single-pulse transfer dynamics

In Fig. 4 we display stop-action movies of single-pulse ejections at different pulse energies with no receiver. At the lowest explored energy, 35 μJ, we observe how, as the laser pulse is absorbed in the donor film, a cavitation bubble is induced due to the partial vaporization of the ink, which expands due to the high pressure within. As the bubble develops, the inner pressure decreases until it is balanced by the outer pressure plus capillary forces. At this point, the external forces overcome the internal ones and the bubble collapses. At higher energies the dynamics is essentially the same but the bubble expands further and an incipient jet appears during collapse. However, this jet does not propagate beyond the furthest front position of the bubble and recedes with its collapse, unlike the common dynamics of the LIFT of low-viscosity Newtonian liquids [14]. In the case of 346 μJ some instabilities can be observed on the bubble tip as it reaches the maximum front position (5 μs), probably due to its fast expansion. At the highest explored energy (692 μJ), the high inner pressure exerts a force on the liquid surface which is capable of overcoming the capillary forces and breaks the bubble walls leading to burst. In this high energy regime a jet is also created. This can travel beyond the bubble apex, however, it does so in a turbulent manner and it breaks up scattering some material. This unstable dynamics sets a maximum gap and energy at which well-defined voxels can be printed: in the conditions of the present experiment this would correspond to a gap of around

1 mm and a pulse energy of 346 μJ. If printing with a larger gap, more energy would be required, which would lead to bubble burst and, thus, deposits with splash and satellites. The observed dynamics clearly contrasts with the typical one of low-viscosity liquids where long stable jets are usually obtained [14].

In Fig. 5a we plot the front position versus time for several energies (35, 69, 104 and 173 μJ). The maxima of the plots in this figure correspond to the furthest front position for each pulse energy. Then, in Fig. 5b we plot each pulse energy versus its corresponding maximum. If we compare this dataset with E_{min} *vs. Gap,* we observe that the points follow a similar trend. In view of this, and considering the dynamic behavior of Fig. 4, it seems reasonable to interpret E_{min} as the pulse energy that is required for the bubble to reach the receiver substrate.

Also from Fig. 5a we can estimate the maximum velocities reached by the bubble front during transfer, obtaining values of around 50, 80, 120 and 150 m/s for each energy in increasing order. These values are comparable to the typical ones usually obtained with both Newtonian [16] and non-Newtonian liquids [26,28]. We can have a rough estimate of the maximum shear rate during bubble expansion through dividing those velocities by the thickness of the wet donor film (80 μm), which leads to values of the order and greater than 10^6 s^{-1} in all cases. Regarding the non-Newtonian behavior of the Ag-SP ink observed in Fig. 1, the estimated shear rate values are much higher than the maximum measurable with our rheometer. Nevertheless, in view of the shear-thinning trend obtained we can assume that viscosities well below 1 Pa·s will be achieved at shear rates around 10^6 s^{-1}. Thus, there is a dramatic decrease in ink viscosity during liquid ejection. As we can observe in Fig. 5a (for energies between 35 and 173 μJ) the initial bubble pressure results in a very high expansion velocity, which translates into a high shear rate and thus the ink becomes less viscous. At these very first moments, with the viscosity substantially reduced, the ink can follow the bubble expansion and flow along the bubble walls. Then, when the bubble expansion slows down the shear rate decreases and the ink becomes more viscous again. This can be linked to the fact that the induced jet does not propel forward but retracts with the bubble. Finally, the bubble totally deflates leaving a protuberance on the donor film. Even though the capillary forces would tend to make the surface more uniform and flat, the bump on the donor film can remain several milliseconds due to the final high viscosity of the ink (as it will be seen later in Section 3.3, Fig. 8). In the case of higher pulse energies (346 and 692 μJ), faster expansion velocities develop, which lead to even lower viscosities, and in turn account for the observed unstable bubble walls, turbulent jet dynamics and burst.

In the full range of explored energies (below 300 μJ), we did not observe a well-defined jet that propels well ahead the bubble front in any case. In consequence, printing should occur through bubble contact. This behavior contrasts with the most common one in LIFT, either using Newtonian or non-Newtonian liquids, in which jetting is usually observed [13-15,25,28]. *Turkoz et al.* [24] and *Kalaitzis et al.* [26] compared in two different works the ejection dynamics in the LIFT of both Newtonian and non-Newtonian liquids. In both experiments the non-Newtonian fluids showed a shear-thinning behavior, however, each one had a slightly different rheology: *Turkoz et al.* used a water-based Xanthan gum solution (without suspended particles) with viscosities around 1 Pa·s at a shear rate of 1 s^{-1}, and *Kalaitzis et al.* a nanoparticle dispersion (particles smaller than 200 nm) of 50 Pa·s at 1 s^{-1}. Regarding the dynamics, they both obtained jets even when using non-Newtonian fluids, which aspect-ratio was smaller than that of Newtonian ones. Since in both cases the fluids rheology was different to ours, the response to shear rate of those inks was also different, which can account for the substantial differences between the behaviors observed in those works (jetting) and ours (practical absence of jetting). Another study performed by *Munoz-Martin et al.* used a high solid content SP ink more similar to ours, in that case especially designed for photovoltaic applications [34]. That ink had a viscosity of around 250 Pa·s at low shear rate (the exact value was not provided in the paper) with silver particles of 1-5 μm in suspension. As in our case, the corresponding transfer dynamics did not result in a jet either, but in a bubble that expanded.

However, in the work of *Munoz-Martin et al.* the wall of the bubble always broke up in a myriad of particles. The ink of our experiment, with a viscosity of 25 Pa·s at a shear rate of 1 s^{-1} and a broad dispersion of particle size (0.3-10 μm), is an intermediate case between that of *Kalaitzis et al.* and that of *Munoz-Martin et al.* The corresponding dynamics, though substantially different from both those works, presents some common elements with them: on one hand, it displays some jetting like in the case of *Kalaitzis et al.* but, on the other, it is dominated by the expansion of a prominent bubble, such in the case of *Munoz-Martin et al*.

The transfer dynamics of single voxels on a receiver substrate was also considered. For the acquisition of the stop-action movies (Fig. 6) we have chosen the same gap (300 μm) as in Fig. 2. At a pulse energy of 52 μJ we can observe how a bubble expands but retracts before reaching the receiver; therefore, there is no transfer, as it was found in the deposits. As we increase the energy to 91 μJ, the bubble contacts the receiver, as we already predicted from the free bubble expansion dynamics, and transfer occurs. Soon after contact, the bubble starts deflating and a bridge between the donor film and the receiver substrate develops. This bridge remains attached to the donor film for a long time since the loss of kinetic energy of the liquid results in an increase of the ink viscosity and the fluid motion is slowed down. Finally, the bridge breaks up after several milliseconds. As we further increase the energy to 121 μJ we observe a faster expansion that leads to an earlier contact of the bubble, essentially following the same pattern as in the previous case. Since the initial induced pressure is higher than before, more material is dragged from the donor film and transferred onto the receiver, leading to a bridge lasting longer.

In the LIFT of liquid donor films, deposition usually takes place through contact of the displaced ink with the receiver substrate before breakup occurs; transfer through a flying droplet is rare [35]. When printing low-viscosity Newtonian liquids, transfer typically occurs through jetting [15,16,21,36]. However, by using narrow gaps and relatively high pulse energies that result in large expanding bubbles, transfer can also occur through direct bubble contact (before the formation of the jet) with the receiver substrate [36,37], as we observe for our high viscosity, non-Newtonian ink in the present work. Nevertheless, long lasting bridges as the ones shown in Fig. 6 are not common in low-viscosity liquids, not even when transfer takes place through bubble contact. However, in a different work, *Turkoz et al.* [38] observed a similar bridging phenomenon, even though they employed a Newtonian low-viscosity (4-7 mPa·s) ink that always exhibited jetting. The main difference between that ink and those of previous works is its prominent viscoelastic behavior. In that work the authors identified two transfer mechanisms: the so-called 'on-contact' mechanism (the jet stretched almost to the maximum before reaching the receiver and rapidly broke up) and 'bridging' (the jet reached the receiver and a long lasting connection with the donor film was created). In our work we never observe a behavior analogous to the 'on-contact' mechanism for the generated bubble, but we do observe the formation of long lasting bridges, although with significant discrepancies respect to the work of *Turkoz et al*. First, as already mentioned, the bridge arises from the collapse of the bubble instead of corresponding to the thinning jet; and, second, the bridge in our experiment lasts considerably longer (around 10 times more) and does not evolve into beads-on-a-string. These differences can be attributed to the different viscosities: whereas *Turkoz et al.* have a low-viscosity Newtonian liquid, we are printing a high-viscosity shear-thinning ink. The shear-dependent viscosity of our ink prevents the jet formation and promotes the long lasting bridge: the dramatic increase in viscosity when the liquid slows down inhibits the onset of the liquid flow along the bubble wall responsible for jetting [14,39] and hampers the bridge thinning necessary for breakup. Furthermore, this impedes the appearance of beads-on-a-string as the bridge slowly thins and, thus, it finally breaks up in a stable manner.

In view of these observations, and in contrast to Newtonian inks, which always exhibit similar transfer behaviors, we observe with these experiments that non-Newtonian inks display substantially different dynamics in function of their rheologies (thinning behavior, viscosity, particle size and distribution), which in turn impact the printing outcomes. In view of this, it seems that in the LIFT of high-viscosity SP inks each different ink will require its dedicated study for optimum printing.

3.3 Line printing and transfer dynamics

Once we printed and characterized single voxels we varied the overlap between adjacent spots in order to obtain continuous lines. With that purpose, we decreased the center-to-center pulse separation from 400 to 100 μm (in steps of 50 μm), by varying the scan speed at a constant repetition rate of 2 kHz (Fig. 7). The energy was set to 104 μJ and the gap to 300 μm in order to properly visualize the transfer dynamics. When using spot separations between 250 and 400 μm we always obtain isolated voxels with an average radius of 125 μm. As we decrease the spot-to-spot separation to 200 μm, we achieve a continuous line, though it is not well defined and shows some scalloping [8,40]. As the overlap is further increased lines become non-continuous. This result is surprising since a shorter distance between spots translates into a greater overlap between deposited voxels, which would be expected to lead to continuous lines with more transferred material [40]. In order to investigate these results, we carried out time-resolved imaging of the ink ejection dynamics during line printing.

In Fig. 8a we can observe the transfer dynamics without any receiver substrate of a single pulse event within a line. We printed at the same conditions as before (2 kHz and 104 μJ) decreasing the center-to-center spot separations: 400, 200 and 100 μm. Since the laser beam is scanned from left to right, on the left side of each frame we can still visualize the modifications remaining on the donor film by the previous shots and, on the right, the transfer event corresponding to the current pulse under study. At a pulse separation of 400 μm we can observe the dynamics corresponding to the free-expanding bubble as seen in Fig. 4, which indicates that there is no interaction between contiguous pulses. In this case, the protuberances on the donor film are visible and well separated. However, for the 200 μm case some interaction starts to be visible. First, the previous pulses on the donor film do not appear as separate entities anymore. Second, we can observe how, at 10 μs and after, the bubble expansion is not symmetrical and the left wall is affected by the previously modified donor film. If we further decrease the spot separation to 100 μm we can notice a large continuous protuberance on the donor film corresponding to previous pulses. The current pulse strongly interacts with the previous ones, which modifies the liquid ejection dynamics, leading even to some bursting (5 μs). In fact, by taking different snapshots at the same delay under identical irradiation conditions, we have observed notable instabilities. Depending on the experiment, and in a random way, the induced bubble expands freely, inflates asymmetrically, bursts or even does not develop at all. Thus, each pulse is strongly influenced by the previous one. Comparing this case to the former one (spot separation larger than 200 μm), the furthest front position in each frame is smaller, which is also due to the interaction between neighboring pulses. As a result, uneven printing takes place (Fig. 8b).

From the stop-action movies we can measure the maximum bubble radius on the donor film: around 225 μm. Thus, we can consider that the area of the donor film that is modified by the laser pulse is delimited by the circumference of the corresponding bubble. Once the bubble has collapsed, this area is no longer flat but presents a bump in the middle, which flattens as we move away from the center. Since for the spot separation of 400 μm the laser pulse is focused outside that region it seems reasonable that the dynamics will be that of a free-expanding bubble as the one observed in Fig. 4. However, for 200 μm, the pulse is focused within the area affected by the expansion of the bubble, but away from the bump. Therefore, since the donor film is quite flat and uniform in the position where the laser pulse impinges, the first moments of expansion do not differ much from a free bubble. However, as the expansion reaches the center of the previous shot, where the bump is located, the bubble wall becomes unstable and asymmetrical on that side. Therefore, there is some interaction between adjacent pulses. In the case of 100 μm the pulse is clearly focused within the affected area (closer to the bump) leading to a stronger pulse-to-pulse interaction. The observed long protuberance along the scanning direction is the result of accumulating successive pulses within previously affected regions, which leads to a non-uniform donor film surface. Since the donor film is not flat anymore, different events such as bubble expansion, bubble burst or no expansion at all can randomly develop depending on the donor film state at the moment of irradiation.

In order to visualize line printing, we placed a receiver substrate at 300 μm from the donor film and performed the same experiment as in Fig. 8. The corresponding stop-action movies of the transfer dynamics of lines are shown in Fig. 9. They reproduce well the dynamics of Fig. 8, the main difference being the presence of connecting bridges that last for a long time (several milliseconds) after each printing event. For a 400 μm separation the bubble expands freely and, since there is no overlap between contiguous pulses, the dynamics corresponds to the single bubble case (Fig. 6). In the case of 200 μm, and according to the explanation provided in the previous paragraph, the printing process appears to be quite repeatable, which is consistent with the morphology of the obtained line (Fig. 9b). For the shortest separation between pulses, 100 μm, the random liquid ejection is evident, which results in clear discontinuities in the printed line (Fig. 9b).

From these observations we can conclude that, in order to successfully print continuous lines, the center-to-center pulse separation has to be of the order or larger than the maximum bubble radius on the donor film. Spot separations smaller than that will result in irregular and even random transfer since there is strong interaction between adjacent bubbles. Also, continuous lines can be achieved if the spot separation is smaller than the printed features diameter. In our experiment both conditions were fulfilled for the 200 μm separation between pulses. In this case, the bubble radius was 225 μm, and the voxel diameter 250 μm. However, scalloping was inevitable since we are working with a non-Newtonian ink and, even though it behaves similarly to a low-viscosity fluid while it transfers, it thickens again once deposited, which prevents the proper liquid coalescence that would lead to a uniform line.

To improve the line quality and avoid these non-uniformities and defects we tried multiple line printing, which consists on printing several lines on top of each other. This is common in printed electronics techniques, especially in IJP, where it serves as an approach to improve the printed features quality, avoiding defects and enhancing line functionality [7]. With that aim, we printed 2 and 3 consecutive layers on top of each other as it is observed in Fig. 7, renewing the donor film before each print. At 2 prints we observe that continuous lines are already obtained at a spot separation of 300 μm, though scalloping is still present. A much stable line is found at 250 μm, whereas bulging appears at 200 μm since instabilities arise when too much liquid is deposited [6,8,40]. For spot separations of 100 and 150 μm discontinuous lines are obtained. We also investigated a third print, for which we obtained continuous lines in all cases except for separations of 100 and 150 μm. While scalloping is found at pulse-to-pulse separations of 400 and 350 μm, and bulging at 200 μm, uniform lines are achieved at 250 μm, and very especially at 300 μm. This proves that multiple printing is a convenient and easy approach for the production of conductive lines that can be used as interconnects in electronic circuits.

4. Conclusions

The study of the LIFT of a highly viscous conductive screen printing ink not only reveals important differences with the LIFT of low-viscosity liquids, extensively analyzed in the literature, but also with other conductive high-viscosity inks. The rhelogical properties of the liquid –not only viscosity, but also particle size and particle size distribution, for instance–, strongly determine the dependence of the printing outcomes with the main process parameters, as well as the dynamics of the transfer process. Therefore, it seems difficult to provide general laws that explain the behavior of a wide range of similar inks; rather, each particular formulation will probably require its own detailed analysis.

The printing of single voxels at different pulse energies and donor-receiver gaps reveals that LIFT is feasible for printing circular droplets in a repeatable way for a wide range of process parameters; the volume of the dried voxels displays a rather linear relationship with pulse energy, especially for low energies and small gaps, with a trend to saturation at high energies. The time-resolved imaging analysis of the same process proves that transfer proceeds in all cases through contact of the bubble with the receiver substrate instead of jetting, as it is common in the LIFT of low-viscosity inks. In fact, jetting is absent, or merely residual, in all the investigated transfer events, which we attribute to the non-Newtonian nature of the ink under study.

The printing of lines through single scan by the overlap of consecutive voxels shows that under the investigated conditions it is not possible to obtain uniform continuous lines, as it would be desirable in the applications. When the distance between adjacent laser pulses is reduced, the line evolves from a set of separate voxels to scalloped continuous lines to, surprisingly, discontinuous lines. The time-resolved imaging analysis indicates that the defects encountered at the smallest separations –completely unexpected– are due to the instabilities in the transfer behavior arising from the alteration of the donor film morphology induced by the previous pulses in the line. However, multiple scan printing allows obtaining uniform continuous lines at some overlaps, which proves the feasibility of LIFT for making interconnects in printed electronics applications with the ink considered in the study.

Acknowledgments

This work was funded by MINECO of the Spanish Government: Project FLASH-PRINT (TEC2015-72425-EXP) and Project LAPER (TEC2017-83301-P). The authors thank Dr. J. Ortín for his assistance in the rheological measurements.

References

[1] Y. Zhang, C. Liu, D. Whalley, Direct-write techniques for maskless production of microelectronics: A review of current state-of-the-art technologies, 2009 ICEPT-HDP (2009) 10894001.

[2] Q. Li, J. Zhang, Q. Li, G. Li, X. Tian, Z. Luo, F. Qiao, X. Wu, J. Zhang, Review of printed electrodes for flexible devices, Front. Mater. 5 (2019) 77.

[3] P. Calvert, Inkjet Printing for Materials and Devices, Chem. Mater. 13 (2001) 3299-3305.

[4] G. Cummins, M.P.Y. Desmulliez, Inkjet printing of conductive materials: a review, Circuit World 38 (2012) 193-213.

[5] A. Lee, K. Sudau, K. H. Ahn, S. J. Lee, N. Willenbacher, Optimization of experimental parameters to suppress nozzle clogging in inkjet printing, Ind. Eng. Chem. Res. 51 (2012) 13195−13204.

[6] J. Stringer, T. M. Althagathi, C.C.W. Tse, V.D. Ta, J.D. Shephard, E. Esenturk, C. Connaughton, T.J. Wasley, J. Li, R. W. Kay, P.J. Smith, Integration of additive manufacturing and inkjet printed electronics: a potential route to parts with embedded multifunctionality, Manufacturing Rev. 3 (2016) 12.

[7] J.F. Salmerón, F. Molina-Lopez, D. Briand, J.J. Ruan, A. Rivadeneyra, M.A. Carvajal, L.F. Capitán-Vallvey, N.F. Derooij, A.J. Palma, Properties and printability of inkjet and screen-printed silver patterns for RFID antennas, J. Electron Mater. 43 (2014) 604-617.

[8] D. Zhu, M. Wu, Highly conductive nano-silver circuits by inkjet printing, J Electron. Mater. 47 (2018) 5133-5147.

[9] D.T. Gethin, E.H. Jewell, T.C. Claypole, Printed silver circuits for FMCG packaging, Circuit World 39 (2013) 188 -194.

[10] M.R. Somalu, A. Muchtar, W. Ramli Wan Daud, N.P. Brandon, Screen-printing inks for the fabrication of solid oxide fuel cell films: A review, Renew. Sust. Energ. Rev. 75 (2017) 426–439.

[11] W.E. Taylor, N. Mardesich, C.F. Gay, The impact of screen printing on the cost of solar cell metallization, J. Sol Energ.-T ASME 102 (1980) 55-58.

[12] K. Reinhardt, N. Hofmann, M. Eberstein, The importance of shear thinning, thixotropic and viscoelastic properties of thick film pastes to predict effects on printing performance, 2017 21st EMPC (2018) 17748964.

[13] P. Serra, A. Piqué, Laser-induced forward transfer: fundamentals and applications, Adv. Mater. Technol. 4 (2019) 1800099.

[14]M. Duocastella, J. M. Fernández-Pradas, J. L. Morenza, P. Serra, Time-resolved imaging of the laser forward transfer of liquids, J. Appl. Phys. 106 (2009) 084907.

[15]C. Boutopoulos, I. Kalpyris, E. Serpetzoglou, I. Zergioti, Laser-induced forward transfer of silver nanoparticle ink: time-resolved imaging of the jetting dynamics and correlation with the printing quality, Microfluid. Nanofluid. 16 (2014) 493-500.

[16]M. Duocastella, J.M. Fernández-Pradas, J.L. Morenza, P. Serra, Sessile droplet formation in the laser-induced forward transfer of liquids: A time-resolved imaging study, Thin Solid Films 518 (2010) 5321-5325.

[17]R.C.Y. Auyeung, H. Kim, S. Mathews, A. Piqué, Spatially modulated laser pulses for printing electronics, Appl. Optics 54 (2015) 31.

[18]T. Inui, R. Mandamparambil, T. Araki, R. Abbel, H. Koga, M. Nogia, K. Suganuma, Laser-induced forward transfer of high-viscosity silver precursor ink for non-contact printed electronics, RSC Adv. 5 (2015) 77942.

[19]A. Palla-Papavlu, M. Filipescu, S. Vizireanu, L. Vogt, S. Antohe, M. Dinescu, A. Wokaun, T. Lippert, Laser-induced forward transfer of hybrid carbon nanostructures, Appl. Surf. Sci. 374 (2016) 312-317.

[20]A. Piqué, H. Kim, R.C.Y. Auyeung, I. Beniam, E. Breckenfeld, Laser-induced forward transfer (LIFT) of congruent voxels, Appl. Surf. Sci. 374 (2016) 42-48.

[21]D. Puerto, E. Biver, A.-P. Alloncle, P. Delaporte, Single step high-speed printing of continuous silver lines by laser-induced forward transfer, Appl. Surf. Sci. 374 (2016) 183-189.

[22]M.I. Sanchez-Aniorte, B. Mouhamadou, A.P. Alloncle, T. Sarnet, P. Delaporte, Laser-induced forward transfer for improving fine-line metallization in photovoltaic applications, Appl. Phys. A 122 (2016) 595.

[23]M. Makrygianni, A. Milionis, C. Kryou, I. Trantakis, D. Poulikakos, I. Zergioti, On-demand laser printing of picoliter-sized, highly viscous, adhesive fluids: Beyond inkjet limitations, Adv. Mater. Interfaces 5 (2018) 1800440.

[24]E. Turkoz, L. Deike, C.B. Arnold, Comparison of jets from Newtonian and non-Newtonian fluids induced by blister-actuated laser-induced forward transfer (BA-LIFT), Appl. Phys. A-Mater. 123 (2017) 652.

[25]E. Turkoz, A. Perazzo, H. Kim, H.A. Stone, C.B. Arnold, Impulsively induced jets from viscoelastic films for high-resolution printing, Phys. Rev. Lett. 120 (2018) 074501.

[26]A. Kalaitzis, M. Makrygianni, I. Theodorakos, A. Hatziapostolou, S. Melamed, A. Kabla, F. de la Vega, I. Zergioti, Jetting dynamics of Newtonian and non-Newtonian fluids via laser-

induced forward transfer: Experimental and simulation studies, Appl. Surf. Sci. 465 (2019) 136–142.

[27] O. Koritsoglou, I. Theodorakos, F. Zacharatos, M. Makrygianni, D. Kariyapperuma, R. Price, B. Cobb, S. Melamed, A. Kabla, F. de la Vega, I. Zergioti, Copper micro-electrode fabrication using laser printing and laser sintering processes for on-chip antennas on flexible integrated circuits, Opt. Mater. Express 9 (2019) 3046-3058.

[28] I. Theodorakos, A. Kalaitzis, M. Makrygianni, A. Hatziapostolou, A. Kabla, S. Melamed, F. de la Vega, I. Zergioti, Laser-Induced Forward Transfer of High Viscous, Non-Newtonian silver nanoparticle inks: jet dynamics and temporal evolution of the printed droplet study, Adv. Eng. Mater. (2019) 1900605 (article in press).

[29] A. Eshkeiti, A.S.G. Reddy, S. Emamian, B.B. Narakathu, M. Joyce, M. Joyce, P. D. Fleming, B. J. Bazuin, M. Z. Atashbar, Screen Printing of Multilayered Hybrid Printed Circuit Boards on Different Substrates, IEEE T. Comp. Pack. Man. 5 (2015) 415-421.

[30] M. Duocastella, M. Colina, J.M. Fernández-Pradas, P. Serra, J.L. Morenza, Study of the laser-induced forward transfer of liquids for laser bioprinting, Appl. Surf. Sci. 253 (2007) 7855-7859.

[31] M.S. Brown, C.F. Brasz, Y. Ventikos, C.B. Arnold, Impulsively actuated jets from thin liquid films for high-resolution printing applications, J. Fluid. Mech. 709 (2012) 341-370.

[32] M. Colina, M. Duocastella, J.M. Fernández-Pradas, P. Serra, J.L. Morenza, Laser-induced forward transfer of liquids: Study of the droplet ejection process, J. Appl. Phys. 99 (2006) 084909.

[33] M. Duocastella, A. Patrascioiu, J.M. Fernández-Pradas, J.L. Morenza, P. Serra, On the correlation between droplet volume and irradiation conditions in the laser forward transfer of liquids, Appl. Phys. A-Mater. 109 (2012) 5-14.

[34] D. Munoz-Martin, C.F. Brasz, Y. Chen, M. Morales, C.B. Arnold, C. Molpeceres, Laser-induced forward transfer of high-viscosity silver pastes, Appl. Surf. Sci. 366 (2016) 389-396.

[35] J.A. Barron, H.D. Young, D.D. Dlott, M.M. Darfler, D.B. Krizman, B.R. Ringeisen, Printing of protein microarrays via a capillary-free fluid jetting mechanism, Proteomics 5 (2005) 4138-4144.

[36] P. Sopeña, J.M. Fernández-Pradas, P. Serra, Laser-induced forward transfer of low viscosity inks, Appl. Surf. Sci. 418 (2017) 530–535.

[37] M. Duocastella, J.M. Fernández-Pradas, J.L. Morenza, P. Serra, Droplet printing through bubble contact in the laser forward transfer of liquids, Appl. Surf. Sci. 257 (2011) 2825–2829.

[38]E. Turkoz, A. Perazzo, L. Deike, H. A. Stone, C. B. Arnold, Deposition-on-contact regime and the effect of donor-acceptor distance during laser-induced forward transfer of viscoelastic liquids, Opt. Mater. Express 9 (2019) 2738-2747.

[39]A. Patrascioiu, J.M. Fernández-Pradas, A. Palla-Papavlu, J.L. Morenza, P. Serra, Laser-generated liquid microjets: correlation between bubble dynamics and liquid ejection, Microfluid. Nanofluid. 16 (2014) 55–63.

[40]C. Florian, F. Caballero-Lucas, J.M. Fernández-Pradas, S. Ogier, L. Winchester, D. Karnakis, R. Geremia, R. Artigas, P. Serra, Printing of silver conductive lines through laser-induced forward transfer, Appl. Surf. Sci. 374 (2016) 265–270.

Figure captions

Figure 1

Plot of the measured stress and viscosity response to shear rate of the silver screen printing ink employed in the experiments. The ink shows a non-Newtonian shear-thinning behavior, with a viscosity varying from 2 to 10^3 Pa·s in the explored shear rate range.

Figure 2

Optical microscopy images of several droplets printed on glass at different laser pulse energies (indicated on the left). The gap is set to 300 μm and the distance between consecutive spots is 500 μm. The feature size increases with the pulse energy. Both columns correspond to the same deposited features: just after printing (wet droplets) and once baked in the oven (dry voxels). The voxel diameter is 15% smaller than the droplet one, and the volume is reduced a factor of 3 as the solvent evaporates.

Figure 3

a) Radius of the printed voxels versus pulse energy for different gaps. The radius increases with pulse energy from a minimum feature size (80 μm) which is almost the same for all gaps. b) Volume of the same printed voxels versus pulse energy. The volume increases with pulse energy with a minimum value of 50 pL which is rather independent of the gap. The continuous lines correspond to a linear fit of eq. 1.

Figure 4

Stop-action movies of the dynamics of single pulse transfer at different pulse energies (indicated on the left) with no receiver substrate. The delay after the laser pulse is indicated on top of the images. As the laser pulse is absorbed (0 μs) a bubble is induced, which expands and retracts with no jet propelling forward. When the energy is too high (692 μJ), the bubble bursts.

Figure 5

a) Front position versus time for different pulse energies as obtained from the time-resolved imaging study of Fig. 4. b) Minimum printing energy versus gap (extracted from Fig. 3a-b), and pulse energy versus the maximum front position (extracted from Fig. 5a).

Figure 6

Stop-action movies of the transfer dynamics of single pulses at different pulse energies (indicated on the left) with a receiver substrate placed at 300 μm. The delay after the laser pulse is indicated on top of the images. The transfer proceeds through bubble contact, creating a bridge between the donor film and the receiver substrate, which breaks after several milliseconds.

Figure 7

Optical microscopy images of consecutive voxels printed at different pulse-to-pulse separations (indicated on the left). The gap is set at 300 μm, the pulse energy at 104 μJ, the repetition rate at 2 kHz and the scan speed is varied accordingly. Multiple printing is considered, applying several layers (displayed on top of the images), in order to obtain uniform lines. Optimum line printing conditions correspond to 3 prints and 300 μm spot-to-spot separation.

Figure 8

a) Stop-action movies of a single pulse LIFT event within a line at different spot separations (indicated on top of the images) at a pulse energy of 104 μJ and with no receiver. The repetition rate is kept at 2 kHz and the laser is scanned from left to right at different speeds. The delay after the laser pulse is indicated on the left side of the images. A red arrow indicates the position of the current pulse. The modifications of the previous pulses are visible on the left of the arrow. b) Images of the deposits corresponding to the same printing conditions when placing a receiver substrate at 300 μm.

Figure 9

a) Stop-action movies of a single pulse LIFT event within a line at different spot separations (indicated on top) at a pulse energy of 104 μJ and a receiver placed at 300 μm. The repetition rate is kept at 2 kHz and the laser is scanned from left to right at different speeds. The delay after the laser pulse is indicated on the left side of the images. A red arrow indicates the position of the current pulse of visualization. The modifications of the previous pulses are visible on the left of the arrow. b) Images of the deposits corresponding to the same printing conditions (receiver substrate at 300 μm).

Figure

Click here to download Figure: 5_Figures_revised.docx

Figure 1

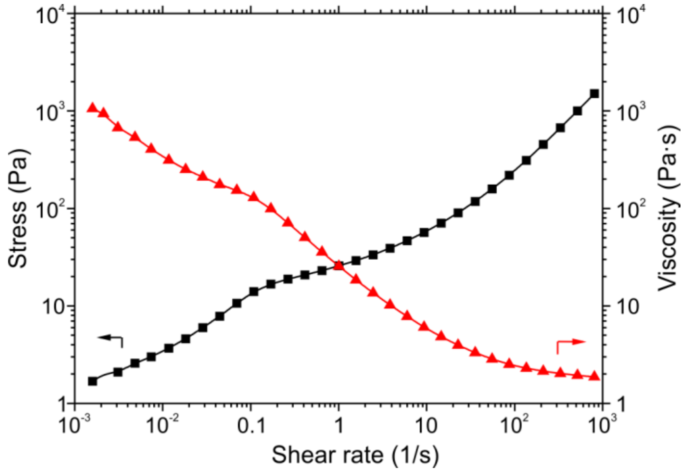

Figure 2

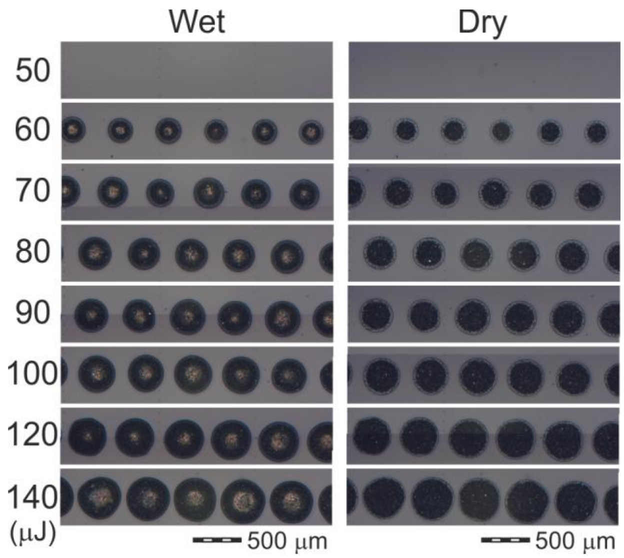

Figure 3

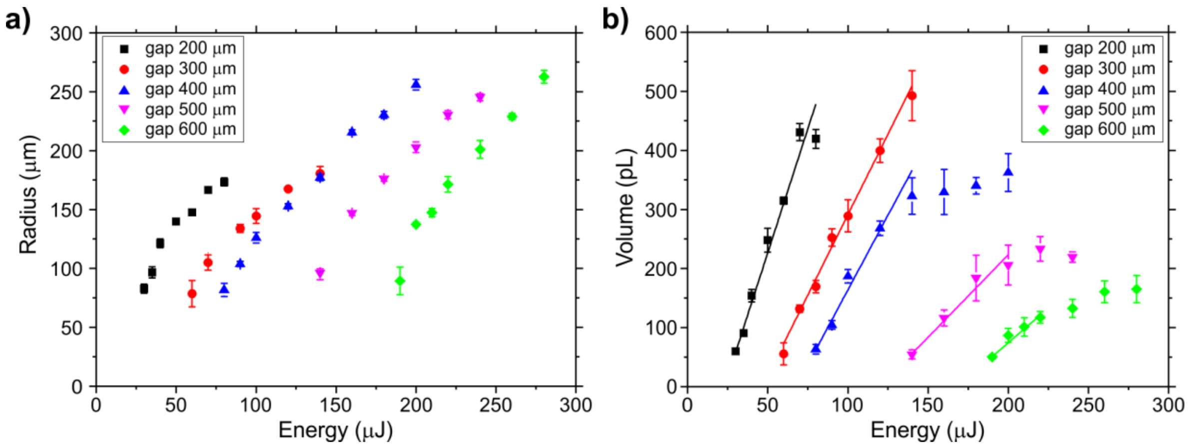

a)
Radius (µm)
Energy (µJ)
gap 200 µm
gap 300 µm
gap 400 µm
gap 500 µm
gap 600 µm
0
50
100
150
200
250
300
b)
Volume (pL)
Energy (µJ)
gap 200 µm
gap 300 µm
gap 400 µm
gap 500 µm
gap 600 µm
0
100
200
300
400
500
600

Figure 4

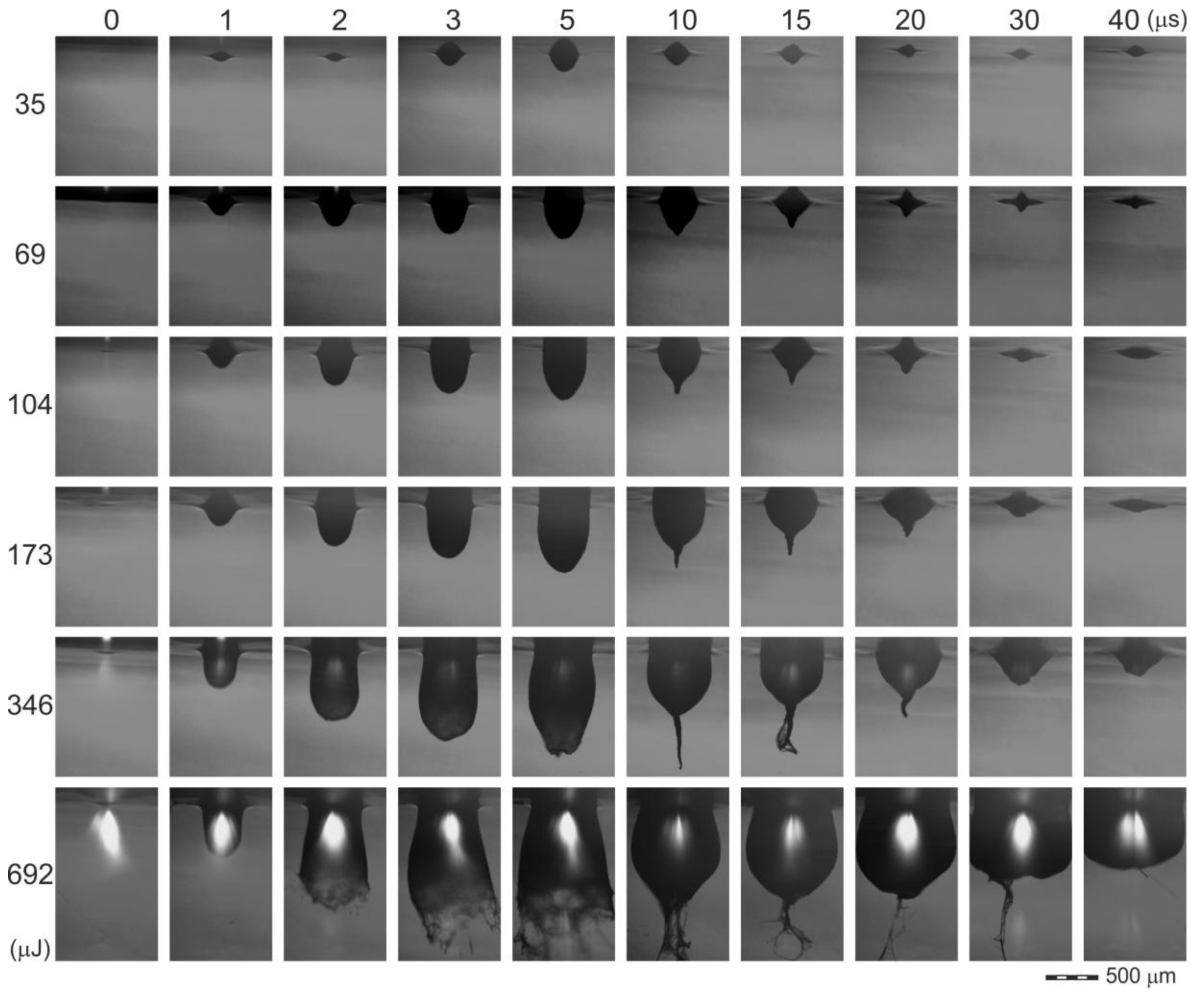

Figure 5

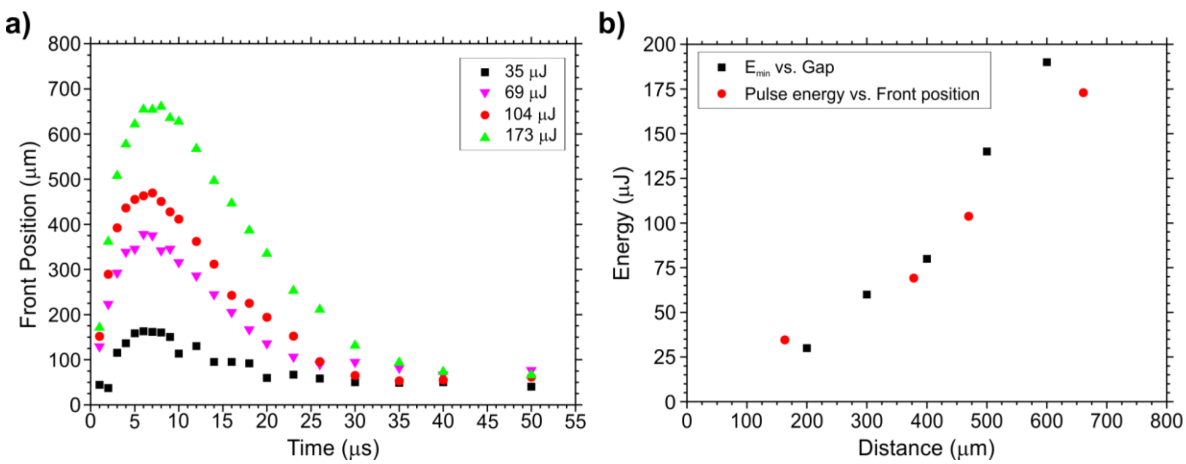
a)
Front Position (μm)
Time (μs)
35 μJ
69 μJ
104 μJ
173 μJ
0
100
200
300
400
500
600
700
800
0
5
10
15
20
25
30
35
40
45
50
55
b)
Energy (μJ)
Distance (μm)
E$_{min}$ vs. Gap
Pulse energy vs. Front position
0
25
50
75
100
125
150
175
200
0
100
200
300
400
500
600
700
800

Figure 6

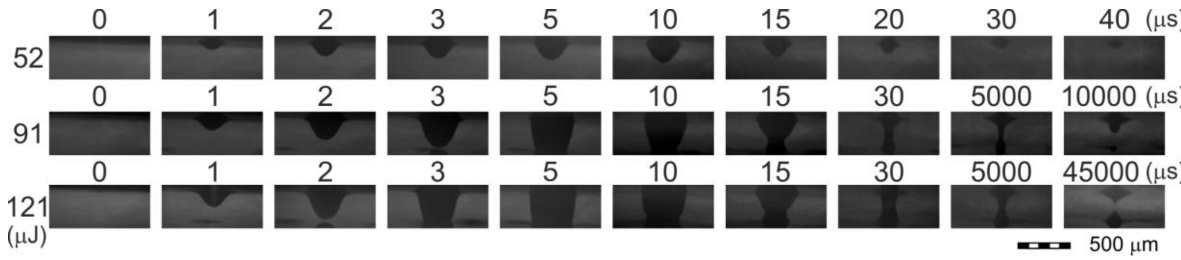
0
1
2
3
5
10
15
20
30
40 (μs)
52
0
1
2
3
5
10
15
30
5000
10000 (μs)
91
0
1
2
3
5
10
15
30
5000
45000 (μs)
121
(μJ)
500 μm

Figure 7

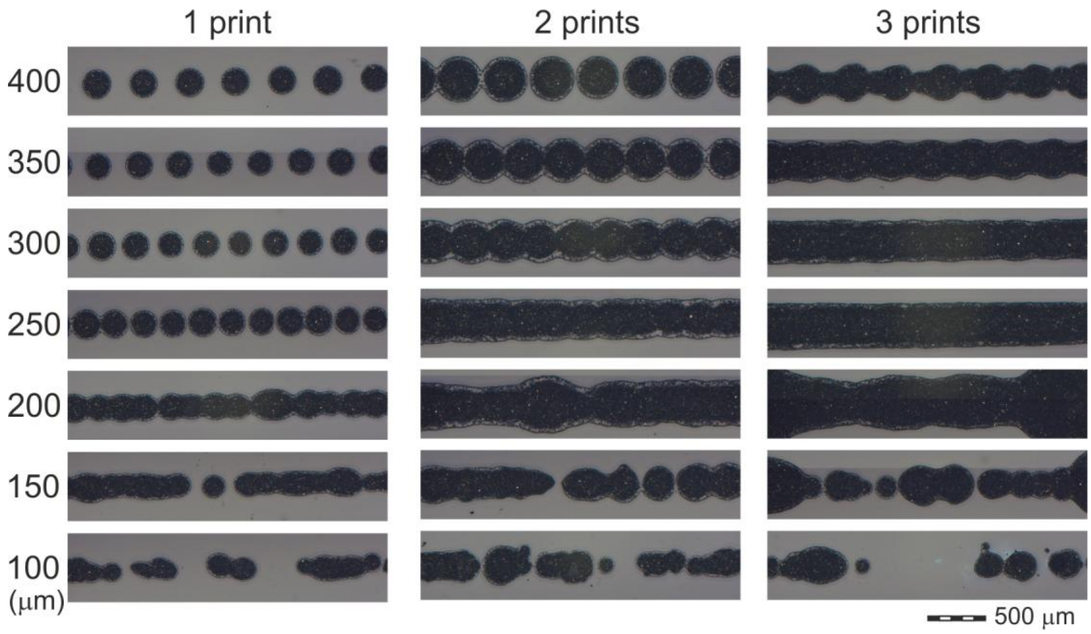

Figure 8

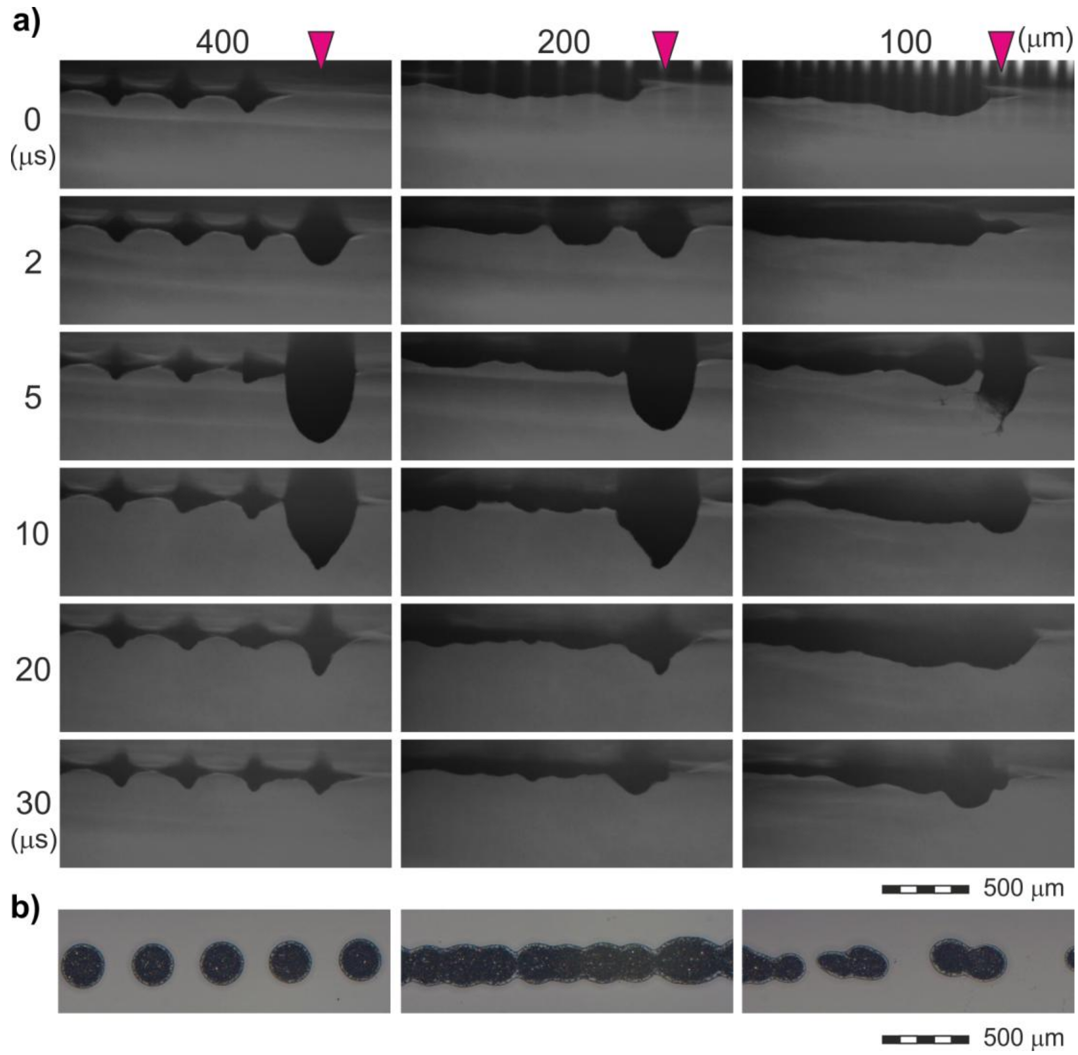

Figure 9

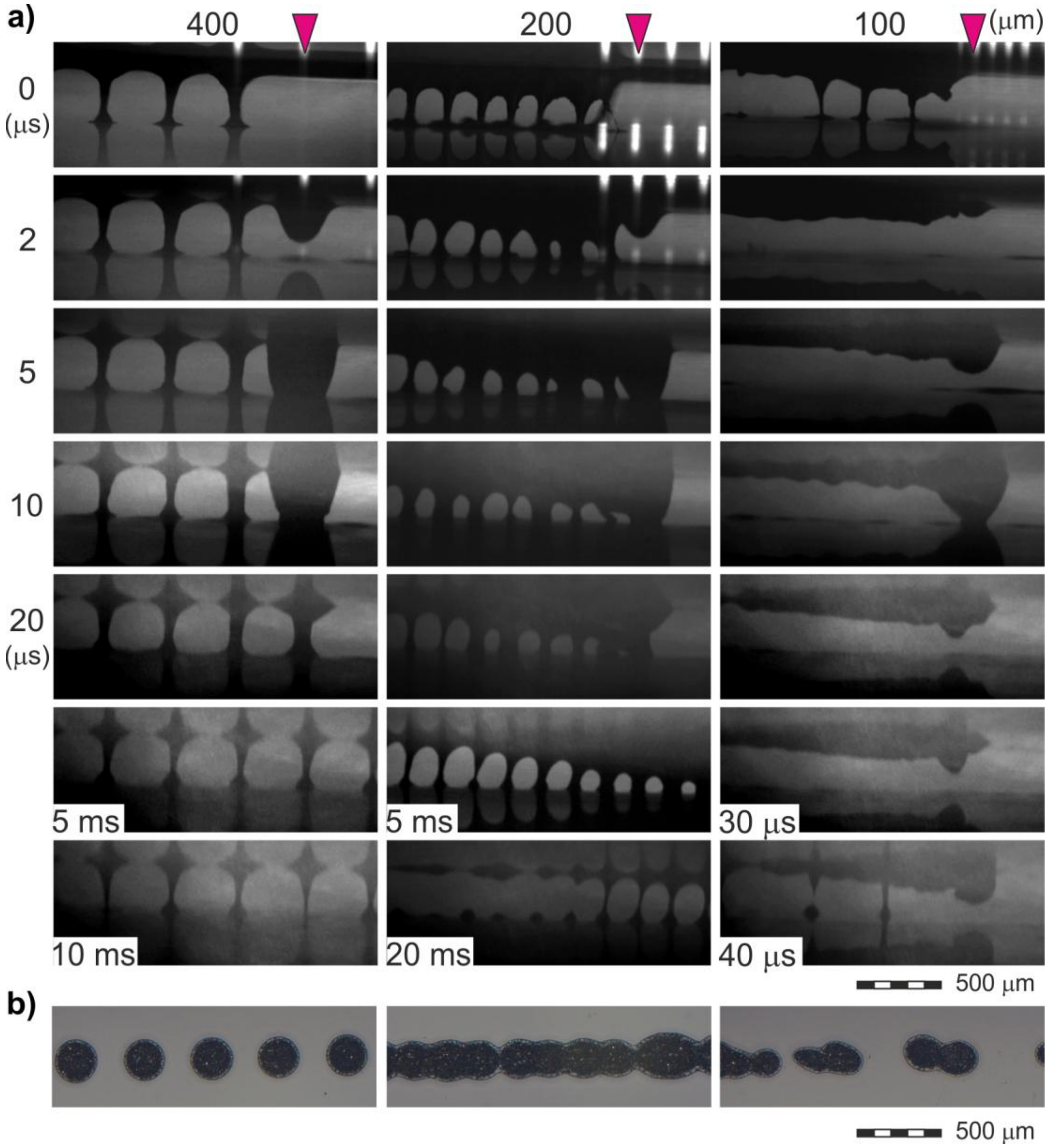

a)
400
200
100
(μm)
0
(μs)
2
5
10
20
(μs)
5 ms
5 ms
30 μs
10 ms
20 ms
40 μs
500 μm
b)
500 μm

Graphical Abstract (for review)

Graphical abstract